

**Modulation of electronic structure of nickel selenide via iron doping for energy-saving hydrogen production coupled with sulfion upgrading**

Shuixiang Xie,<sup>a,1</sup> Xiaojun Wang,<sup>a,1</sup> Yuhuan Li,<sup>a</sup> Shijie Liu,<sup>a</sup> Jiahui Qian,<sup>a</sup> Yuhan Zhang,<sup>a</sup> Linling Jiang,<sup>a</sup> Zhe Cao,<sup>a</sup> Zhenhao Yan,<sup>a</sup> Xiaoyu Wan,<sup>a</sup> Zhaohang Yang,<sup>a</sup> Longhua Zou,<sup>\*b</sup> Wei Zhang,<sup>\*a</sup> and Rui-Qing Li<sup>\*a</sup>

<sup>a</sup> School of Textile and Clothing, Nantong University, Nantong 226019, PR China.

E-mail: liruiqing@ntu.edu.cn; zhangwei@ntu.edu.cn

<sup>b</sup> College of Food and Biological Engineering, Chengdu University, Chengdu 610106, China

E-mail: zoulonghua@cdu.edu.cn

## **Experimental section**

### **Chemicals**

$\text{Ni}(\text{NO}_3)_3 \cdot 6\text{H}_2\text{O}$ ,  $\text{Fe}(\text{NO}_3)_3 \cdot 6\text{H}_2\text{O}$ ,  $\text{NH}_4\text{F}$ ,  $\text{CO}(\text{NH}_2)_2$  and selenium powder were provided from Aladdin.  $\text{Na}_2\text{S} \cdot 9\text{H}_2\text{O}$ ,  $\text{NaBH}_4$  and  $\text{NaOH}$  were purchased from Sinopharm Group and Adamas-beta<sup>®</sup>. Nickel foam (NF) was supplied by Taiyuan source of power company.

### **Synthesis of Fe-Ni<sub>0.85</sub>Se**

The growth of Fe-Ni<sub>0.85</sub>Se on the surface of NF was accomplished via hydrothermal and selenization reaction processes. Initially, 1.6 mmol  $\text{Ni}(\text{NO}_3)_2$ , 0.4 mmol  $\text{Fe}(\text{NO}_3)_3$ , 10 mmol  $\text{CO}(\text{NH}_2)_2$ , 6 mmol  $\text{NH}_4\text{F}$  were added in 35 mL water under the agitation to form uniform solution, and the NF put into in above solution, which was heated at 120 °C for 6 h to obtain the NiFe LDH precursor. Then, the NiFe LDH precursor was placed in an autoclave containing 0.118 g selenium powder and 5 mL  $\text{NaBH}_4$ , which was heated up to 140 °C for 12 h to synthesize Fe-Ni<sub>0.85</sub>Se. For comparison, the Ni<sub>0.85</sub>Se was also fabricated under similar conditions except for the absence of  $\text{Fe}(\text{NO}_3)_3$ .

### **Materials characterization**

The crystal phases, morphologies, microstructures, elemental mapping and chemical states of catalysts were analyzed by X-ray diffraction (XRD, Bruker D8), scanning electron microscopy (SEM, FIB-SEM GX4), transmission electron microscopy (TEM, FEI Tecnai G20) and X-ray photoelectron spectrometer (XPS, Thermo ESCALAB 250Xi), respectively.

### **Electrochemical measurements**

The electrochemical tests were performed on the electrochemical workstation (CHI 760E) with a standard three-electrode system using the as-fabricated samples as the working electrodes. The polarization curves were recorded at a scan of 2 mV s<sup>-1</sup> to analyze catalytic performances. The electrochemical impedance spectroscopy was tested in the frequency range of 10<sup>-1</sup>-10<sup>5</sup> Hz. The double layer capacitances was obtained utilizing cyclic voltammetry (CV) method with various applied potentials from 0.2 to 0.3 V.

### **Theoretical calculations.**

All spin polarized DFT calculations were carried out using the Perdew-Burke-Ernzerhof (PBE) functional with DFT-D3 correction as implemented in the Vienna *ab initio* simulation package (VASP 5.4).<sup>1-4</sup> A plane-wave basis set with energy cut-off of 450 eV was employed within the framework of projector augmented-wave (PAW) method.<sup>5</sup> The Brillouin zone was sampled using a Monkhorst–Pack  $2 \times 2 \times 1$  k-points mesh. Gaussian smearing with a smearing width of 0.2 eV was used. A  $3 \times 3$  supercell, four layers of pristine Ni<sub>0.85</sub>Se (111) and Fe-Ni<sub>0.85</sub>Se (111) surface were chosen to construct the investigated models. The bottom two layers were fixed, while the top two layers and the adsorbates were allowed to relax. A vacuum region of 15 Å was added to avoid interaction between neighboring layers. All the atoms were allowed to relax until the maximum Hellman-Feynman force on each atom was less than 0.02 eV·Å<sup>-1</sup>, except the atoms on the boundary which were fixed in all directions. The Gibbs free energy (*G*) values of the adsorbed species were calculated by using the equation:  $G = E + ZPE - TS$ , where *G*, *E*, *ZPE* and *TS* represent the free energy, total energy from DFT calculations, zero-point energy and entropic contributions (*T* was set to be 298.15 K), respectively. The adsorption energy (*E*<sub>ads</sub>) of species *M* is calculated by formula of  $E_{\text{ads}} = E_{\text{M/slab}} - E_{\text{M}} - E_{\text{slab}}$ , where *E*<sub>M</sub>, *E*<sub>slab</sub> and *E*<sub>M/slab</sub> represent total energy of free molecule, clean substrate and adsorbed complex between them. With this definition, a negative value of *E*<sub>ads</sub> means a thermodynamically preferred adsorption process. To investigate the kinetic processes of H<sub>2</sub>O dissociation, climbing image nudged elastic band (CI-NEB) method was employed to trace the minimum energy pathways (MEPs) and locate its transitional state (TS).<sup>6,7</sup> The TS was verified with a single imaginary frequency.

The oxidation of S<sup>2-</sup> into S<sub>8</sub> proceeds in the following steps:<sup>8-10</sup>





The asterisk (\*) designates the reaction surfaces of Ni<sub>0.85</sub>Se and Fe-Ni<sub>0.85</sub>Se covered by a layer of sulfur atoms. The symbols S\*, S<sub>2</sub>\*, S<sub>3</sub>\*, S<sub>4</sub>\*, and S<sub>8</sub>\* represent the models featuring the respective chemisorbed species on the reaction surfaces.

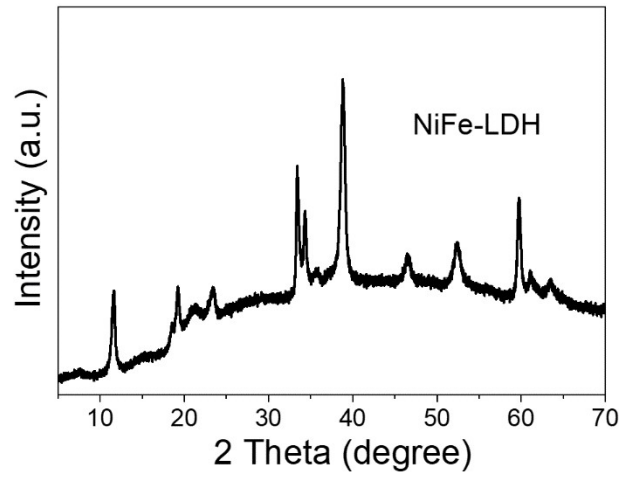


**Fig. S1** XRD pattern of NiFe LDH precursor. Several characteristic diffraction peaks confirm the formation of NiFe LDH.

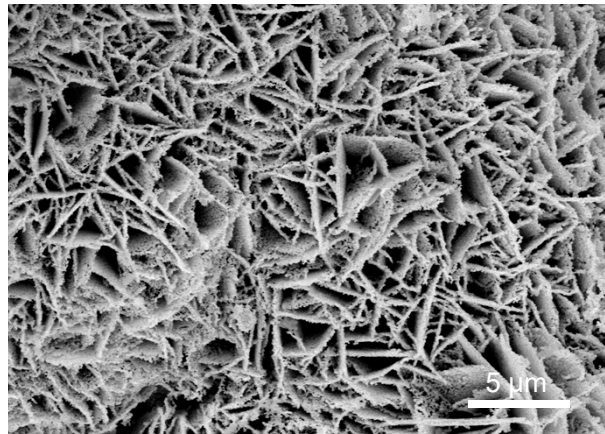


**Fig. S2** SEM image of Fe-Ni<sub>0.85</sub>Se. The Fe-Ni<sub>0.85</sub>Se possesses similar nanosheets morphology.

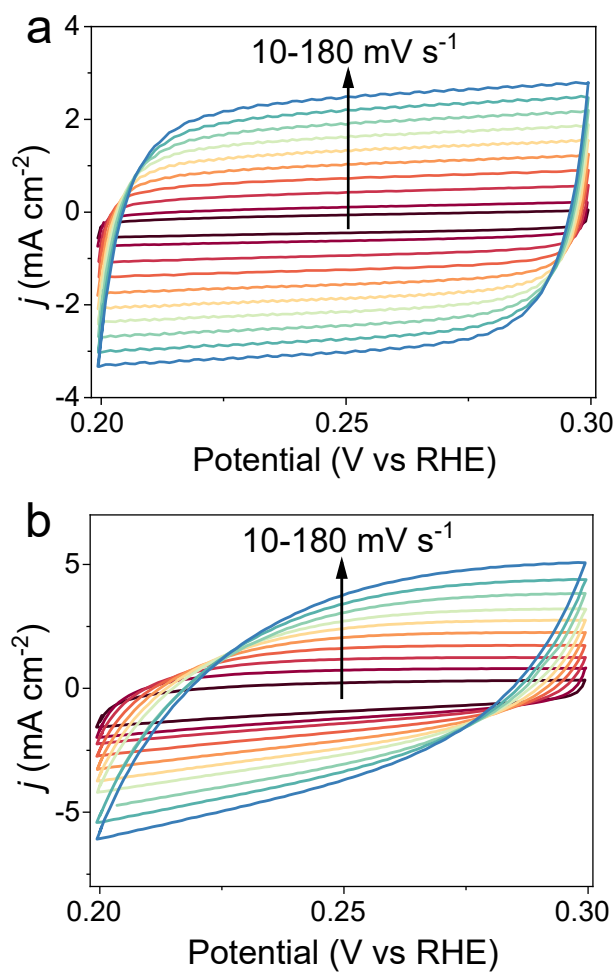


**Fig. S3** Cyclic voltammetry curves at various scanning rates for (a) Ni<sub>0.85</sub>Se and (b) Fe-Ni<sub>0.85</sub>Se. Non-Faradaic scans show that the Fe-Ni<sub>0.85</sub>Se has higher capacitive tendency than the Ni<sub>0.85</sub>Se.

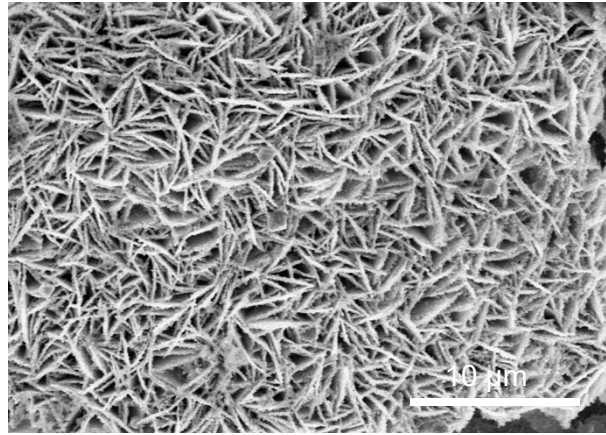


**Fig. S4** SEM image of Fe-Ni<sub>0.85</sub>Se after the HER measurement. SEM image of Fe-Ni<sub>0.85</sub>Se after the HER stability shows well-maintained nanosheets morphology.

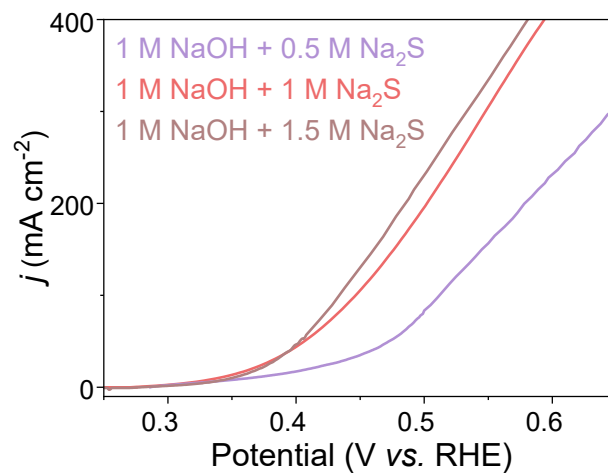


**Fig. S5** LSVs of Fe-Ni<sub>0.85</sub>Se for SOR in 1.0 M NaOH with various concentrations of Na<sub>2</sub>S.

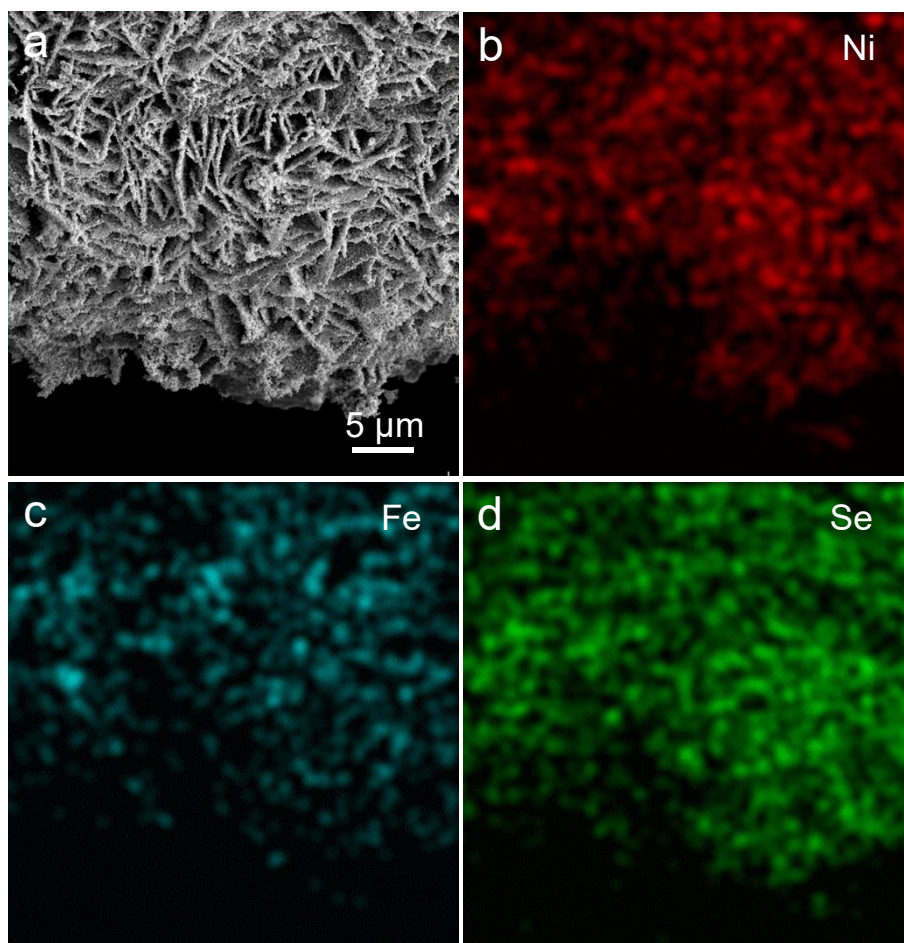


**Fig. S6** SEM and homologous element mapping images of Fe-Ni<sub>0.85</sub>Se after the HER measurement. These images show uniform distribution of Ni, Fe and Se elements over the Fe-Ni<sub>0.85</sub>Se nanosheets.

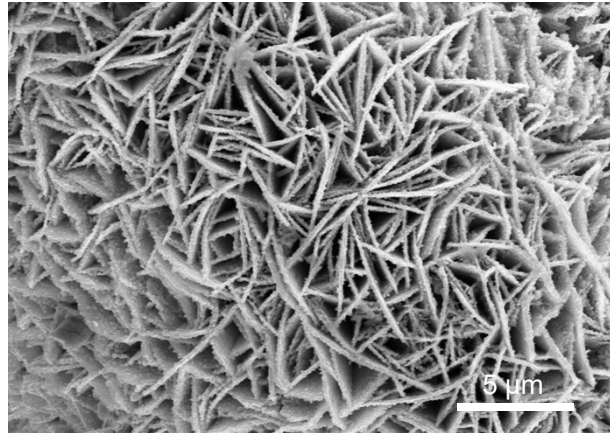


**Fig. S7** SEM image of Fe-Ni<sub>0.85</sub>Se after the SOR measurement. SEM image of Fe-Ni<sub>0.85</sub>Se after the SOR stability shows well-maintained nanosheets morphology.

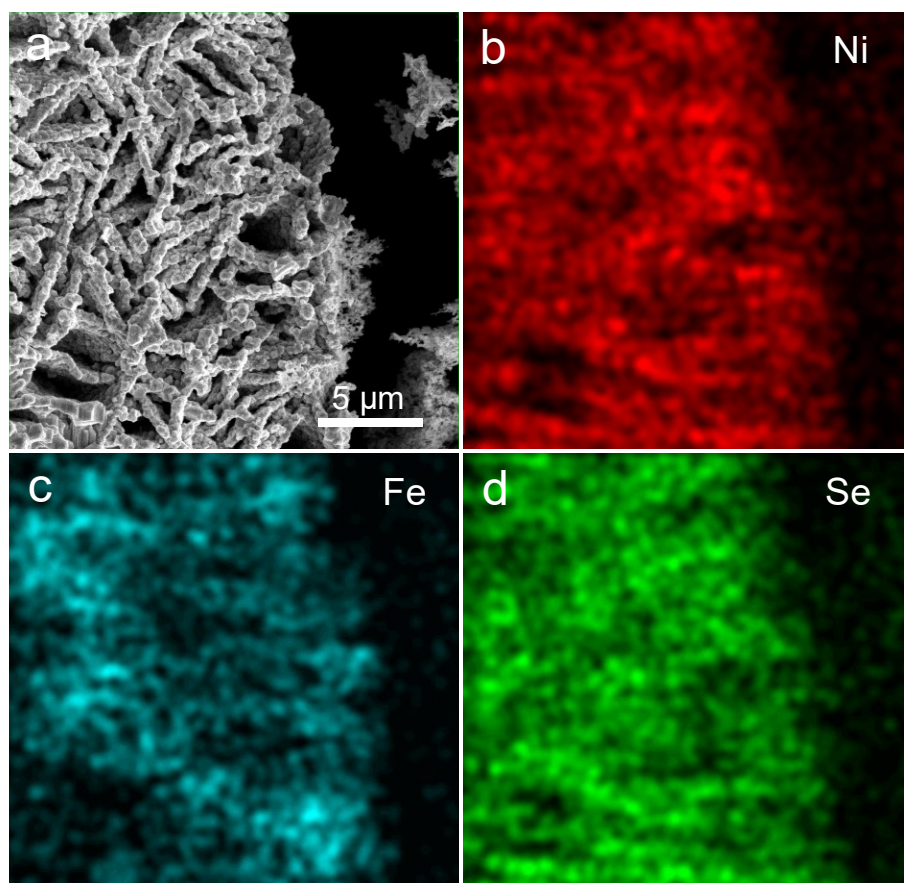


**Fig. S8** SEM and homologous element mapping images of Fe-Ni<sub>0.85</sub>Se after the SOR measurement. These images show uniform distribution of Ni, Fe and Se elements over the Fe-Ni<sub>0.85</sub>Se nanosheets.

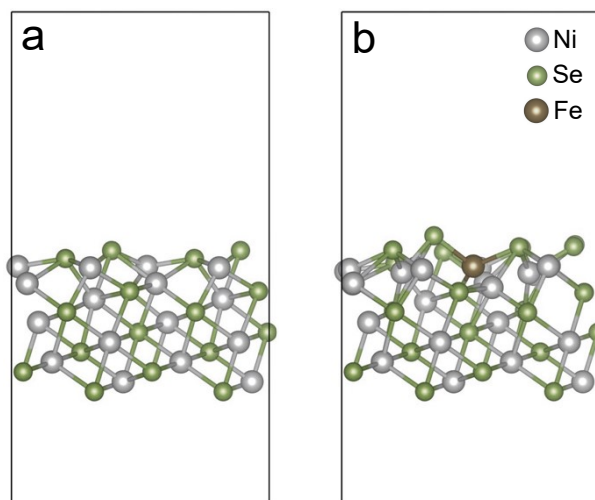


**Fig. S9** Structural models of (a)  $\text{Ni}_{0.85}\text{Se}$  and (b)  $\text{Fe-Ni}_{0.85}\text{Se}$ .

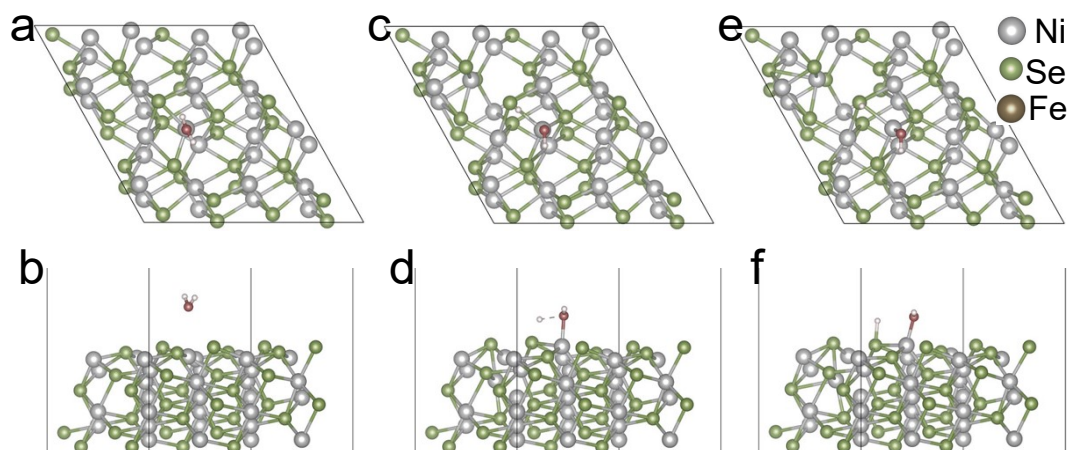


**Fig. S10** Structural evolution models of  $\text{H}_2\text{O}$  dissociation on the  $\text{Ni}_{0.85}\text{Se}$ . As we know, the HER in alkaline media mainly includes three steps: the initial  $\text{H}_2\text{O}$  adsorption, the  $\text{H}_2\text{O}$  adsorption to generate intermediate  $\text{H}^*$ , and final  $\text{H}_2$ . Small  $\text{H}_2\text{O}$  dissociation energy guarantees effective  $\text{H}^*$  production on catalyst, which is significant for subsequent reaction. Fig. S9 shows the dissociation process of  $\text{H}_2\text{O}$  molecule on the  $\text{Ni}_{0.85}\text{Se}$  to produce  $\text{H}^*$  intermediate and Ni acts as active site to dissociate  $\text{H}_2\text{O}$  molecule (Fig. 10c, 10d).

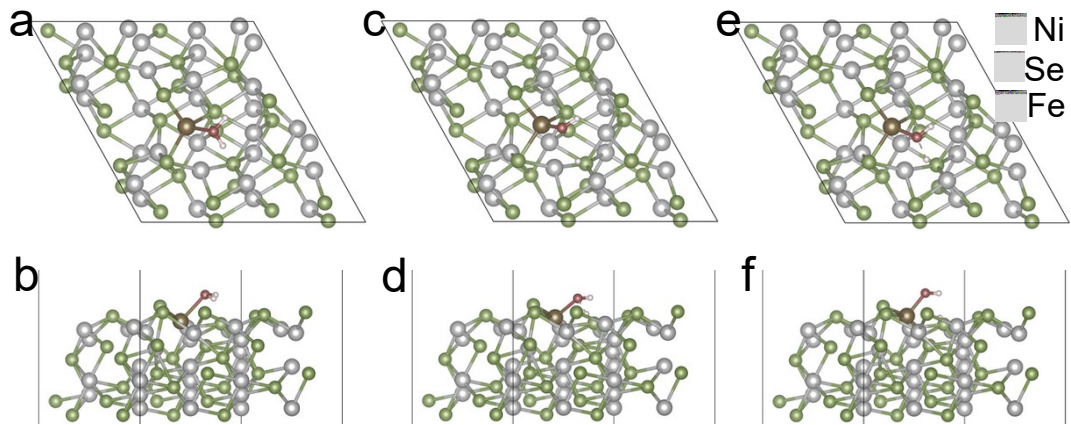


**Fig. S11** Structural evolution models of  $\text{H}_2\text{O}$  dissociation on the  $\text{Fe-Ni}_{0.85}\text{Se}$ . Fig. S11 shows the adsorption and dissociation process of  $\text{H}_2\text{O}$  molecule on the  $\text{Fe-Ni}_{0.85}\text{Se}$  to generate  $\text{H}^*$  intermediate and Fe acts as active site to dissociate  $\text{H}_2\text{O}$  molecule with low dissociation energy barrier (Fig. 11c, 11d).

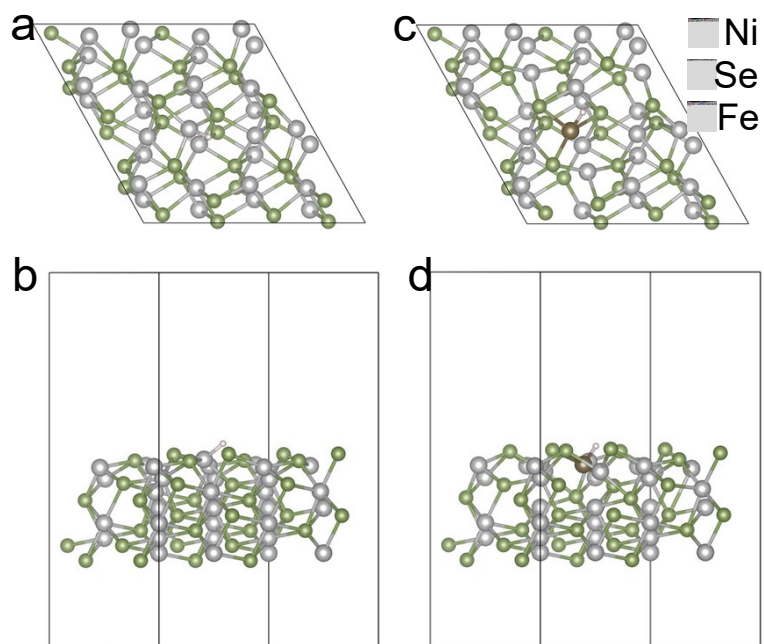


**Fig. S12** Structural evolution models of H\* adsorption on the Ni<sub>0.85</sub>Se (a,b) and Fe-Ni<sub>0.85</sub>Se (c,d). Generally, a moderate value of  $\Delta G_{H^*}$  is beneficial to the HER and neither too strong nor too weak binding would favor the HER process. To reveal the pivotal role of introducing Fe, the  $\Delta G_{H^*}$  values were calculated based on structural evolution models of Ni<sub>0.85</sub>Se (Fig. S12a, S12b) and Fe-Ni<sub>0.85</sub>Se (Fig. S12c, S12d).

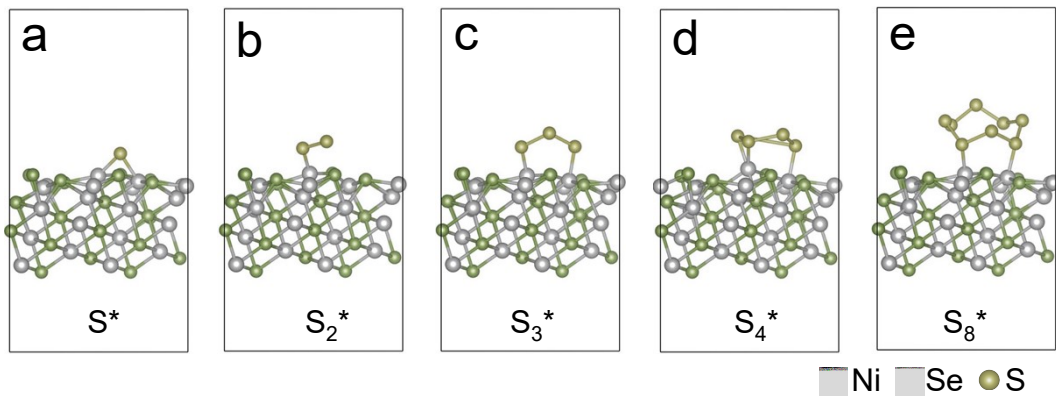


**Fig. S13** Structural evolution of SOR intermediates adsorbed on the  $\text{Ni}_{0.85}\text{Se}$ . Fig. S13 shows structural adsorption model of  $\text{S}^*$  (Fig. S13a),  $\text{S}_2^*$  (Fig. S13b),  $\text{S}_3^*$  (Fig. S13c),  $\text{S}_4^*$  (Fig. S13d), and  $\text{S}_8^*$  (Fig. S13e) on the  $\text{Ni}_{0.85}\text{Se}$  and corresponding calculated free energy changes were calculated.

**Table S1** The comparison of HER performance of Fe-Ni<sub>0.85</sub>Se with developed catalysts.

Catalysts	Overpotential at 10 mA cm <sup>-2</sup> (mV)	Stability (h)	Reference
<b>Fe-Ni<sub>0.85</sub>Se</b>	<b>114</b>	<b>50</b>	<b>This work</b>
NiFeP/SG	115	30	S11
Co-Fe <sub>2</sub> P	117	22	S12
Ti <sub>3</sub> CN(OH) <sub>x</sub> /MoS <sub>2</sub>	120	10	S13
MC-M <sub>2</sub> C/PNCDs	121	24	S14
Ni <sub>2</sub> P-Ni <sub>5</sub> P <sub>4</sub>	128	48	S15
Al-Ni <sub>2</sub> P/TM	129	20	S16
c-NiP <sub>2</sub> /m-NiP <sub>2</sub>	134	14	S17
P-CoNi <sub>2</sub> S <sub>4</sub>	135	40	S18
Ni-N <sub>3</sub>	139	14	S19
MoS <sub>2</sub> /CeO <sub>2</sub>	147	200	S20
Co-BNCNTs	155	20	S21
1T-MoS <sub>2</sub>	158	24	S22
N,O-carbon	161	24	S23
CoP	173	--	S24
Co <sub>1</sub> Mn <sub>1</sub> CH/NF	180	10	S25
Mn-Ni <sub>2</sub> P/NiFe LDH	184	20	S26
WS <sub>2</sub> -NSs	214	14	S27
MoS <sub>2</sub>	248	10	S28
Ni <sub>1.5</sub> Fe <sub>0.5</sub> P	282	--	S29
Co <sub>0.25</sub> Fe <sub>0.75</sub> -LDH	365	8	S30

**Table S2** The comparison of SOR performances of Fe-Ni<sub>0.85</sub>Se with reported catalysts.

Catalysts	Potential (V) at 10 mA cm <sup>-2</sup>	Stability (h)	Reference
<b>Fe-Ni<sub>0.85</sub>Se</b>	<b>0.340</b>	<b>20</b>	<b>This work</b>
Ni-MoS <sub>2</sub> /SM	0.35	~22	S31
HEDP-Rh	0.385	20	S32
v-NiS <sub>2</sub>	0.41	4	S33
IrO <sub>2</sub>	0.43	--	S34
WS <sub>2</sub> NSs	0.48	1	S35
V <sub>Pd</sub> -Pd <sub>4</sub> S MNRS/CP	0.511	20	S36
SP-RhIene	0.550	30	S37
PdCo/C	0.69	--	S38
TiO <sub>2</sub> /GC	0.77	--	S39
CoS	0.90	--	S40

## References

1. J. P. Perdew, K. Burke and M. Ernzerhof, *Phys. Rev. Lett.*, 1996, **77**, 3865.
2. S. Grimme, *J. Comput. Chem.*, 2010, **27**, 1787.
3. G. Kresse and J. Furthmüller, *Physical Review B*, 1996, **54**, 11169.
4. G. Kresse and J. Furthmüller, *Comp.mat.er.sci*, 1996, **6**, 15-50.
5. G. J. Kresse and D. Joubert, *From Ultrasoft Pseudopotentials to the Projector Augmented-Wave Method*, 1999.
6. G. Henkelman, *J. Chem. Phys.*, 2000, **113**, 9901.
7. G. Henkelman and H. Jónsson, *J. Chem. Phys.*, 2000, **113**, 9978.
8. S. Semwal, R. Shakir, J. Karthikeyan, A. Sinha and U. Ojha, *ACS Appl. Nano Mater.*, 2023, **6**, 18945.
9. D. He, P. Yang, K. Yang, J. Qiu and Z. Wang, *Adv. Funct. Mater.*, 2024, **34**, 2407601.
10. L. Zhang, Z. Wang and J. Qiu, *Adv. Mater.*, 2022, **34**, 2109321
11. R. Li, B. Wang, T. Gao, R. Zhang, C. Xu, X. Jiang, J. Zeng, Y. Bando, P. Hu, Y. Li and X. Wang, *Nano Energy*, 2019, **58**, 870.
12. S. Wang, P. Yang, X. Sun, H. Xing, J. Hu, P. Chen, Z. Cui, W. Zhu and Z. Ma, *Appl. Catal. B-Environ.*, 2021, **297**, 120386.
13. J. Jiang, F. Li, S. Bai, Y. Wang, K. Xiang, H. Wang, J. Zou and J. Hsu, *Nano Res.*, 2023, **16**, 4656.
14. X. Lu, L. Yu, J. Zhang and X. Lou, *Adv. Mater.*, 2019, **31**, 1900699.
15. L. Wu, L. Yu, F. Zhang, B. McElhenny, D. Luo, A. Karim, S. Chen and Z. Ren, *Adv. Funct. Mater.*, 2021, **31**, 2006484.
16. H. Du, L. Xia, S. Zhu, F. Qu and F. Qu, *Chem. Commun.*, 2018, **54**, 2894.
17. Q. Fu, X. Wang, J. Han, J. Zhong, Z. Tongrui, T. Yao, C. Xu, T. Gao, S. Xi, C. Liang, L. Xu, P. Xu and B. Song, *Angew. Chem., Int. Ed.*, 2021, **133**, 263.
18. X. Lu, S. Zhang, W. Sim, S. Gao and X. Lou, *Angew. Chem. Int. Ed.*, 2021, **133**, 23067.
19. W. Zang, T. Sun, T. Yang, S. Xi, M. Waqar, Z. Kou, Z. Lyu, Y. Feng, J. Wang, S. Pennycook, *Adv. Mater.*, 2021, **33**, 2003846.
20. R. Li, C. Wang, S. Xie, T. Hang, X. Wan, J. Zeng and W. Zhang, *Chem. Commun.*,

- 2023, **59**, 11512.
21. R. Li,, X. Xu, J. Zeng, X. Zhang, X. Wan, S. Guo, X. Wang, S. Xie, Z. Cao, Y. Zhang, C. Wang, J. Deng, O. Fontaine, M. Ge, J. Dai, G. Zhang, W. Zhang, X. Wang and Y. Zhu, *Nano Lett.*, 2025, **25**, 4, 1272.
  22. X. Guo, E. Song, W. Zhao, S. Xu, W. Zhao, Y. Lei, Y. Fang, J. Liu and F. Huang, *Nat. Commun.*, 2022, **13**, 5954.
  23. Q. Liu, S. Sun, L. Zhang, Y. Luo, Q. Yang, K. Dong, X. Fang, D. Zheng, A. Alshehri and X. Sun, *Nano Res.*, 2022, **15**, 8922.
  24. J. Xie, H. Liu, Y. Zhen, Y. Dong, R. Luan, N. Yu, D. Liu, Y. Chai and B. Dong, *J. Colloid Interf. Sci.*, 2022, **614**, 84.
  25. T. Tang, W. Jiang, S. Niu, N. Liu, H. Luo, Y. Chen, S. Jin, F. Gao, L. Wan and J. Hu, *J. Am. Chem. Soc.*, 2017, **139**, 8320.
  26. B. Sang, Y. Liu, X. Wan, S. Xie, G. Zhang, M. Ge, J. Dai, W. Zhang and R. Li, *Chem. Commun.*, 2023, **59**, 8743.
  27. L. Yi, Y. Ji, P. Shao, J. Chen, J. Li, H. Li, K. Chen, X. Peng and Z. Wen, *Angew. Chem. Int. Ed.*, 2021, **60**, 21550.
  28. B. Chen, P. Hu, F. Yang, X. Hua, F. Yang, F. Zhu, R. Sun, K. Hao and Z. Yin, *Small*, 2023, **19**, 2207177.
  29. H. Huang, C. Yu, C. Zhao, X. Han, J. Yang, Z. Liu, S. Li, M. Zhang and J. Qiu, *Nano Energy*, 2017, **34**, 472.
  30. S. Naik, J. Theerthagiri, F. Nogueira, S. Lee, A. Min, G. Kim, G. Maia, L. Pinto and M. Choi, *ACS Catal.*, 2023, **13**, 1477.
  31. F. Liu, X. Cai, Y. Tang, W. Liu, Q. Chen, P. Dong, M. Xu, Y. Tan and S. Bao, *Energy Environ. Mater.*, 2024, **7**, e12644.
  32. Z. Wang, G. Yang, P. Tian, X. Li, K. Deng, H. Yu, Y. Xu, H. Wang and L. Wang, *Chem. Eng. J.*, 2023, **473**, 145147.
  33. S. Zhang, Q. Zhou, Z. Shen, X. Jin, Y. Zhang, M. Shi, J. Zhou, J. Liu, Z. Lu, Y. Zhou and H. Zhang, *Adv. Funct. Mater.*, 2021, **31**, 2101922.
  34. M. Zhang, J. Guan, Y. Tu, S. Chen, Y. Wang, S. Wang, L. Yu, C. Ma, D. Deng and X. Bao, *Energy Environ. Sci.*, 2020, **13**, 119.

35. L. Yi, Y. Ji, P. Shao, J. Chen, J. Li, H. Li, K. Chen, X. Peng and Z. Wen, *Angew. Chem. Int. Ed.*, 2021, **60**, 21550.
36. W. Wang, Q. Mao, S. Jiang, K. Deng, H. Yu, Z. Wang, Y. Xu, L. Wang and H. Wang, *Appl. Catal. B-Environ.*, 2024, **340**, 123194.
37. H. Wang, Y. Liang, S. Liu, X. Mu, H. Yu, K. Deng, Z. Wang, Y. Xu and L. Wang, *Inorg. Chem. Front.*, 2023, **10**, 5686.
38. K. Kim and J. Han, *Int. J. Hydrogen Energy*, 2015, **40**, 4567.
39. P. Sahoo, K. Kim, J. Lee, J. Han and Y. Oh, *ACS Sustain. Chem. Eng.*, 2015, **3**, 1764.
40. K. Kim, J. Son and J. Han, *Int. J. Hydrogen Energy*, 2014, **39**, 10493.